NUMERICAL MODELLING OF ADDITIVELY MANUFACTURED AND WROUGHT MARAGING STEEL TARGETS UNDER BALLISTIC IMPACT

MAISIE EDWARDS-MOWFORTH[1,2], MIGUEL COSTAS[3], MARTIN KRISTOFFERSEN[3,4], TORE BØRVIK[3] & FILIPE TEIXEIRA-DIAS[1]
[1]Institute for Infrastructure and Environment, University of Edinburgh, UK
[2]IMPETUS Afea AS, Flekkefjord, Norway
[3]Structural Impact Laboratory (SIMLab), Norwegian University of Science and Technology, Norway
[4]Multiconsult AS, Tromsø, Norway

ABSTRACT

The advantages of on-demand production and customised or optimised parts make additive manufacturing (AM) an exciting prospect for optimised armour systems. High-strength maraging steel is a martensitic steel, widely used in aerospace and tooling industries. The combination of high-strength and the flexibility of AM gives maraging steel significant potential for impact protection applications. However, the enhanced strength of maraging steel, achieved through heat-treatment, simultaneously causes reduced fracture elongation and impact toughness. Therefore, the improved ballistic perforation resistance comes at a compromise of reduced ductility, with the effects of AM fabrication potentially exacerbating the brittle behaviour. This study predicts the ballistic performance of heat-treated AM maraging steel targets, in comparison to wrought targets of the same material, through simulations validated by experiment data. Numerical models calibrated from material characterisation tests are established in the IMPETUS Afea Solver. The ballistic limit velocity was estimated conservatively within the experimentally determined value for both AM and wrought maraging steel with good agreement. Comparisons are drawn concerning how well the numerical failure techniques implemented, node splitting and element erosion, were able to capture the fragmentation behaviour of the brittle heat-treated, high-strength targets.

Keywords: ballistic impact, maraging steel, additive manufacture, numerical modelling, fragmentation.

1 INTRODUCTION

As additive manufacturing (AM) brings the advantages of on-demand production and customised or optimised parts to the defence industry, important questions arise regarding the structural integrity of safety-critical AM components in armour systems [1]–[4]. Laser powder-bed fusion (LPBF), whereby metallic powder is selectively fused by an energy source to build a part, is one promising AM technology where the uncertainty in resulting material properties has hindered its application in protective structures. The nature of layer-by-layer fabrication, with large thermal gradients in the substrate, can induce discontinuities in the microstructure leading to anisotropy [5], [6]. Printing defects such as porosity, lack of fusion between melt layers and microsegregation, frequently reported, can lead to tendencies for brittle fracture and fragmentation during an impact event [7].

Excessive fragmentation of high-strength AM maraging steel, produced by LPBF, under ballistic impact has recently been evidenced in experimental campaigns [7], [8]. Maraging steel is a martensitic steel, widely used in aerospace and tooling industries, with a low carbon composition that makes it suited to AM through LPBF techniques [6]. Ultra high-strength is achieved after heat-treatment through the development of intermetallic precipitates. The combination of high-strength and the flexibility of AM gives maraging steel significant potential for impact protection applications. AM maraging steel in its as-printed state has been found to exhibit similar ballistic performance to wrought maraging steel of the same

WIT Transactions on The Built Environment, Vol 215, © 2025 WIT Press
www.witpress.com, ISSN 1743-3509 (on-line)
doi:10.2495/SUSI250121

composition [8]. However, the precipitates responsible for enhancement of strength in heat-treated material simultaneously cause reduced fracture elongation and impact toughness [5]. Therefore, a compromise must be sought between improved ballistic perforation resistance and reduced ductility, which may be further exacerbated by AM fabrication defects, as shown by Costas et al. [7].

Numerical models form an important part of the research and design process into new materials in armour systems, especially where the possibility arises for optimisation of geometries and materials. Achieving accurate finite element (FE) simulations of ballistic impact on high-strength AM maraging steel poses two key challenges: firstly, including the effects of AM processing appropriately in material models and, secondly, capturing the fragmentation. A commonly used technique to model failure in explicit simulations, element erosion or deletion, may lead to unrealistic results for large amounts of fragmentation due to the loss of mass in the model. Success has been found with an alternative method in place of element erosion in several studies [9], [10], namely, node splitting: a technique whereby cracks are propagated by separating elements rather than removing elements, which is implemented in the IMPETUS Solver [11].

This study evaluates the performance of numerical models using various failure techniques to predict the ballistic performance of AM maraging steel targets in comparison to wrought targets of the same material. Material models calibrated from material characterisation tests are established in the IMPETUS Solver. Node splitting technology is used to simulate material failure in both the AM maraging steel targets and the APM2 (armour piercing) projectile, in comparison to element erosion. The results of bullet core residual velocity obtained from the simulations are compared with experimental ballistic impact tests, as well as a qualitative analysis of the perforation processes. Comparisons are drawn concerning how well the numerical techniques implemented were able to capture the fragmentation behaviour of the brittle, high-strength targets.

2 EXPERIMENTAL BACKGROUND

The numerical work in this study draws on experimental tests carried out by the authors in a proof-of-concept examination of the ballistic performance of AM and wrought maraging steel. Material characterisation tests, including quasi-static and dynamic tensile tests, and ballistic impact tests were carried out on AM and wrought maraging steel, both before and after an industry standard heat-treatment procedure, using experimental facilities at the Norwegian University of Science and Technology (NTNU). A summary of the main results from the ballistic impact tests, relevant for comparison to numerical models in this study, follows. For a full description of the AM processing, experimental set-ups and results, the reader is referred to Edwards-Mowforth et al. [8].

The experimental ballistic impact tests were conducted in a 16 m^3 chamber by firing APM2 bullets at 2 × 5 mm heat-treated cylindrical target plates, depicted in Fig. 1, using a smooth-bored Mauser rifle. As shown in Fig. 2, fragmentation was present in the target during impact for both the AM and wrought maraging steel, but much more significantly for the former. The extensive fragmentation in the AM material may be attributed to anisotropy and lack of fusion defects induced by the AM processing. In addition, the AM material post heat-treatment was capable of breaking the hard steel core of the armour piercing bullet in each test, whereas this occurred to a lesser extent for the wrought maraging steel, despite both exhibiting similar ballistic limit velocities. Fragmentation in both the target and projectile plays a large role in the perforation mechanisms and therefore requires consideration in numerical models of the impact.

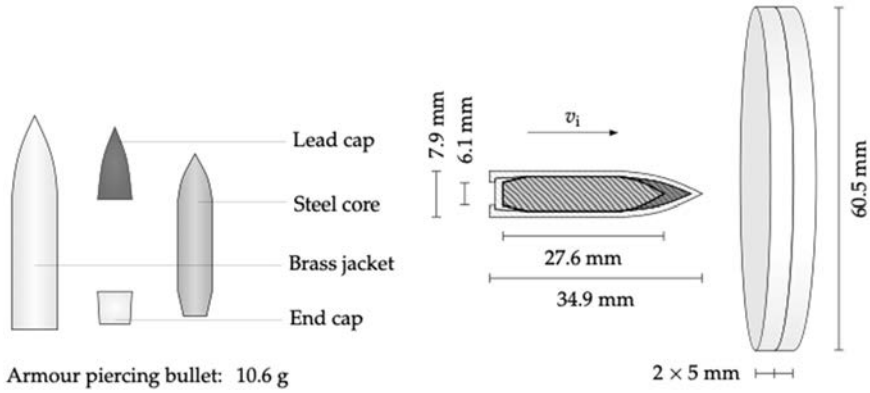

Figure 1: Experimental ballistic impact test set-up. Components of the APM2 bullet (left) and section view of the projectile with 2 × 5 mm heat-treated target plates (right).

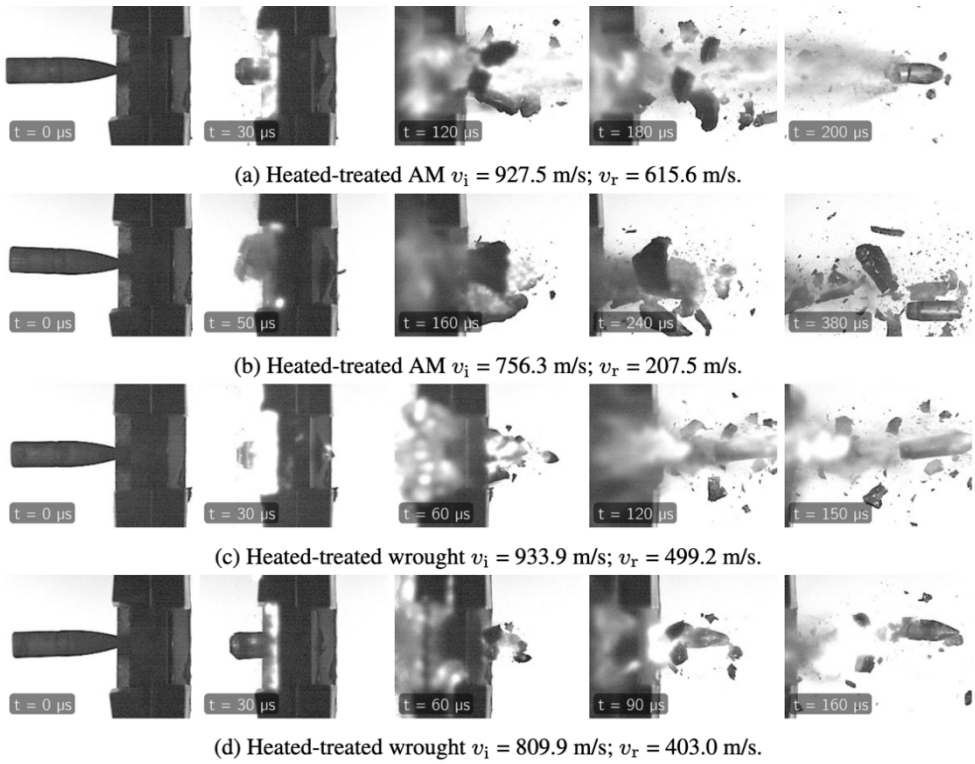

Figure 2: Sequential images of ballistic impact experiments capture with a high-speed camera. Two different impact velocity examples are shown for AM, (a) and (b), and wrought, (c) and (d), heat-treated maraging steel target plates.

3 NUMERICAL SIMULATIONS

3.1 Material modelling

The modified Johnson–Cook (MJC) model is a widely used phenomenological relation for metallic materials under large deformations, high strain rates and high temperatures [12]. Having proved reliable in numerous studies on ballistic impact and AM materials [13]–[15], MJC is also utilised in this study to model the maraging steel target plates and components of the APM2 projectile. The same models were chosen for both target materials to evaluate how well the AM material behaviour could be captured using standard modelling techniques. Empirical parameters to populate the MJC model were calibrated through inverse modelling of the quasi-static tensile tests taken from 0° and 90° to the build direction in the case of the AM maraging steel, and from quasi-static axial compression tests for the APM2 steel bullet core. The AM maraging steel exhibited little anisotropy in work hardening, therefore an average best fit between the calibration at 0° and 90° to the build direction was used [8].

The Cockcroft–Latham (CL) criterion [17] was used to include damage in the model for relative simplicity, requiring only one tensile test to calibrate the CL failure parameter, W_c. The CL parameters were extracted from simulations of quasi-static tensile tests using the calibrated work hardening parameters for each material variation, identifying the critical element at the point of failure. The final value of W_c was averaged from all tests for each material variation. A similar procedure was used for the AMP2 bullet core from simulation of a Brazilian tensile test, using the work hardening calibration obtained from the axial compression test calibration. Crack propagation in the node splitting formulation is defined by the fracture energy parameter, G, taken as a typical value of 5,000 kJ/m^2 for steel [18]. The calibrated work hardening and failure parameters used are reported in Table 1. The typical values for the component materials of the APM2 bullet and maraging steel listed in Fig. 3 were assumed from the literature [8], [13], [16].

Table 1: MJC work hardening parameters for the AM and wrought heat-treated maraging steel, calibrated from quasi-static tensile tests.

	Yield stress	Strain hardening				Strain rate	Failure
	A (MPa)	$Q1$ (MPa)	$C1$	$Q2$ (MPa)	$C2$	C	W_c (MPa)
AM	1,678.7	−73.8	75.9	354.0	200.8	0.0077	170
Wrought	1,730.0	178.7	4.4	120.1	200.0	0.0077	1,274.5

3.2 Numerical set-up

Simulations of the experimental ballistic impact tests were carried out in the explicit FE code IMPETUS Solver. The Ø60.5 mm maraging steel target plates were discretised into elements of approximately 0.1 mm within a Ø15 mm impact zone region, and around 50 elements over the 5 mm target plate thickness, as shown in Fig. 3. A sufficiently small element size consistent with the mesh used for material model calibrations was ensured, as per a computational cell approach [19], while maintaining computational efficiency. Simulations were carried out using both a structured mesh, generated within IMPETUS, and an unstructured mesh, using the open source Gmsh software [20]. As shown in Fig. 3, the resulting unstructured mesh has non-uniform element sizes and shapes. Irregular element

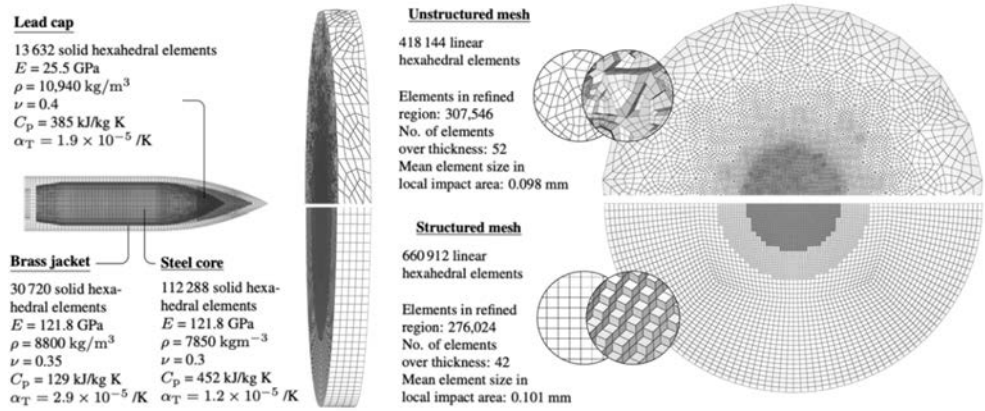

Figure 3: Ballistic impact simulation set-up detailing the mesh specifications for each component, as well as thermoelastic and adiabatic heating constants. The APM2 bullet mesh is displayed to the left, and the target plate to the right shows a half-cut plate of the unstructured and structured mesh types.

sizes were intended to minimise any influence of mesh uniformity on crack patterns of the plate, and to introduce stochastic variation, given that the CL criterion is mesh dependent. The brass jacket, lead cap and bullet core of the APM2 projectile were discretised with regular meshes of 30,720, 13,632 and 71,824 elements, respectively, as also depicted in Fig. 3.

The bullet model was assigned initial velocities to replicate the experimental tests. A frictionless, surface-to-surface, penalty stiffness-based contact algorithm was employed to define interaction between all parts including self-contact, as a conservative assumption. Boundary conditions were representative of the clamp set-up in experimental tests. All components were discretised by solid linear hexahedral elements with selectively reduced integration. Node splitting with the crack plane orthogonal to the direction of maximum principal stress was used as the penalty for reaching the failure criterion and was compared to repeated simulations using element erosion.

3.3 Simulation results

The initial velocity, v_i, and residual velocity, v_r, of the projectile were extracted from the simulations and fitted to the Recht–Ipson model [21] to estimate the ballistic limit velocity, v_{bl} for each material configuration. The Recht–Ipson model is given as

$$v_r = a(v_i^p - v_{bl}^p)^{1/p} \tag{1}$$

where a and p are constants fixed at 1 and 2, respectively, for the purpose of clear comparison. The resulting ballistic limit curves and v_{bl} values for AM and wrought heat-treated maraging steel are shown in Fig. 4 and listed Table 2, respectively.

Using an unstructured mesh with node splitting achieved a v_{bl} value within 2% and 3% of the experimental values for AM and wrought targets, respectively, as shown in Fig. 4. Table 2 reports these v_{bl} values alongside the corresponding results for the structured mesh

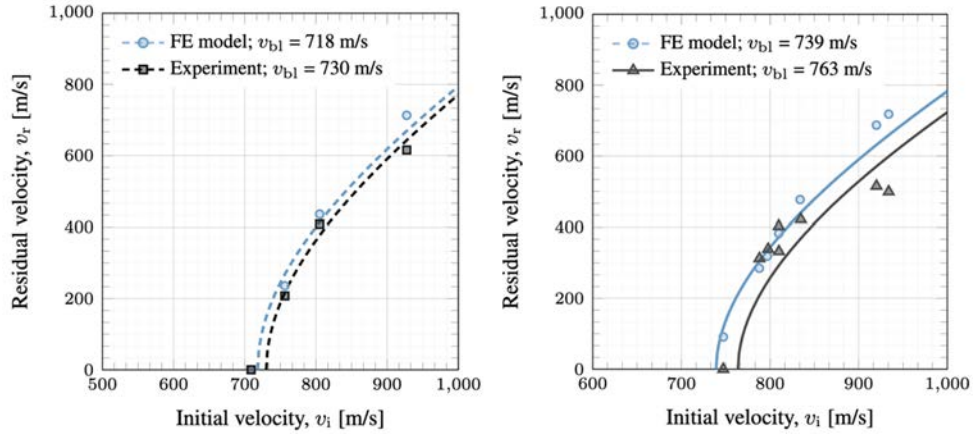

Figure 4: Experimental ballistic impact curves in comparison to simulation predictions using node splitting and the unstructured mesh for (a) AM and (b) wrought heat-treated maraging steel.

Table 2: Ballistic limit velocity for different failure modelling approaches and structured and unstructured meshes for AM and wrought heat-treated maraging steel.

	Node splitting Unstructured mesh v_{bl} (m/s)	Node splitting Structured mesh v_{bl} (m/s)	Element erosion Unstructured mesh v_{bl} (m/s)	Experiment v_{bl} (m/s)
AM	718.2	703.4	636.5	730.1
Wrought	739.1	728.5	820.6	763.3

and element erosion. Using node splitting with a structured mesh achieved a slightly larger, 4% and 5%, difference from the experimental v_{bl} values for AM and wrought targets, respectively. The percentage difference increased to approximately 13% and 11%, respectively, using element erosion. The increase in deviation from the experimentally determined value for the latter may be attributed to the shortfalls of the element erosion technique to capture target fragmentation, found to be significant for the heat-treated maraging steel, especially so for the AM material.

Differences in the capability of node splitting and element erosion to capture target plate fragmentation are documented qualitatively in Fig. 5, which shows the projectile-exit face of the target plates post-perforation. Photos of the perforated experimental test target are also shown in Fig. 5 alongside the corresponding simulation results. For the AM example, a large, irregular shaped perforation channel is shown both for the experiment and from the node splitting simulation with both mesh types, whereas the hole created by element erosion is smaller, evidence of less fragmentation and cracking than that observed in the experiment. For the wrought example, all simulation variations capture a small, circular shaped perforation channel, while only the node splitting simulations capture the radial cracks visible in the experiment. The simulated cracks, however, do not reach the edge of the target plate as they are seen to do in the experiment. This may be partially attributed to the gradual

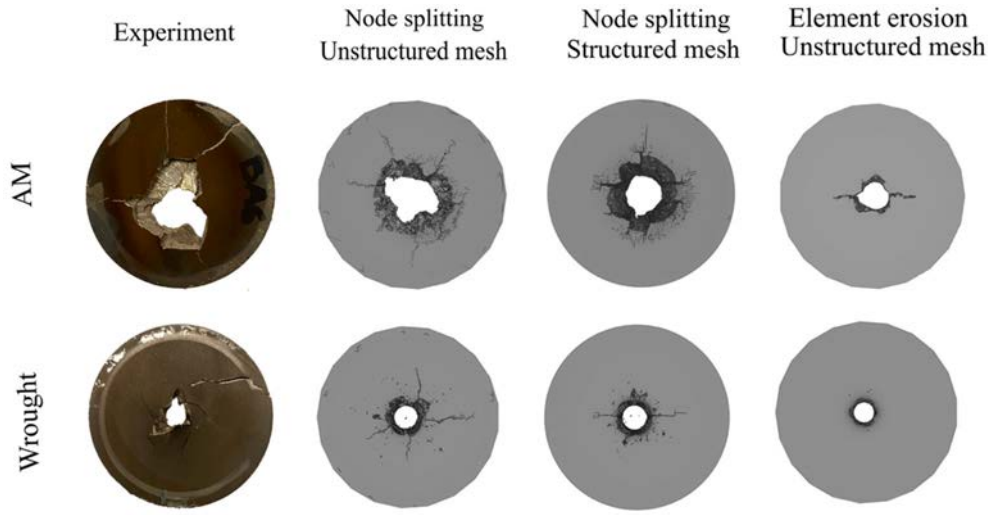

Figure 5: Projectile-exit face of the heat-treated AM (v_i = 756.5 m/s) and wrought (v_i = 933.9) maraging steel target plates impacted by armour piercing bullets: Experiment compared to simulations using different failure techniques and meshes.

increase in element size outside the impact zone prematurely arresting crack growth. Cracks simulated by the node splitting algorithm appear to follow the straight mesh-lines in the structured mesh, whereas the crack patterns appear more natural for the unstructured mesh.

Snapshots throughout the simulated perforation process are displayed in Fig. 6, which further provide evidence of differences between the node splitting and element erosion technique. For both the AM and wrought examples (Figs 6(b) and 6(d)) element erosion appears to generate fewer, smaller fragments compared to the node splitting simulations (Figs 6(a) and 6(c)), resulting in a higher residual velocity of the bullet core after perforation. The simulation with element erosion for the wrought material was the only example in which the hard steel bullet core fragmented, however this did not occur for the corresponding velocity in the experiment, as shown in Fig. 2(c).

Several differences between simulation and experiment in the projectile response were identified in all cases, including with node splitting. The brass jacket was removed during perforation in the experiments on the AM material, but remained in place in the simulations, which were also unable to capture breakages in the bullet core. However, the lack of fragmentation in the bullet core did not induce significantly or hinder accurate ballistic limit velocity predictions. This could indicate that target plate fragmentation is more influential to residual velocity than bullet core fragmentation. Nevertheless, accurate modelling of bullet core fracture requires further experimental tests and validation to improve the failure model.

4 CONCLUSIONS

- Commonly used constitutive models and failure criteria, along with node splitting in the IMPETUS Solver, were able to accurately predict the ballistic limit velocity of heat-treated AM and wrought maraging steel target plates impacted by APM2 projectiles.

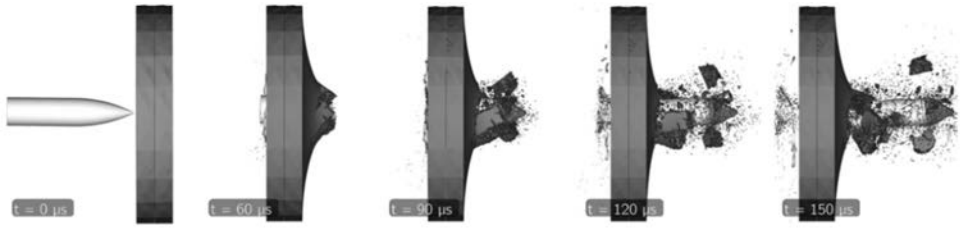

(a) Node-splitting, heat-treated AM, $v_i = 756.5$ m/s; $v_r = 264.5$ m/s.

(b) Element erosion, heat-treated AM, $v_i = 756.5$ m/s; $v_r = 468.2$ m/s.

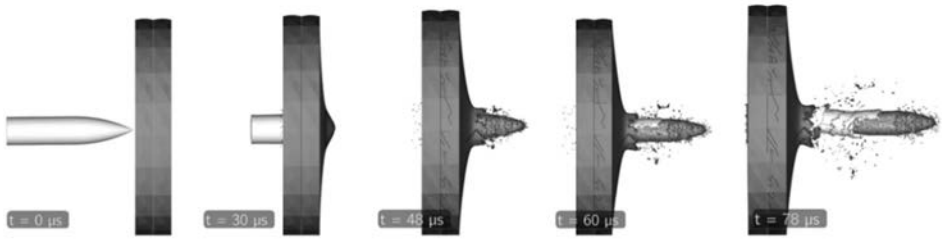

(c) Node-splitting, heat-treated wrought $v_i = 933.9$ m/s; $v_r = 716.5$ m/s.

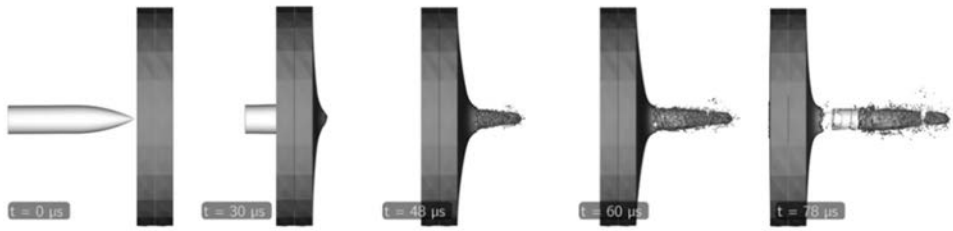

(d) Element erosion, heat-treated wrought $v_i = 933.9$ m/s; $v_r = 684.5$ m/s.

Figure 6: Sequential images throughout simulations of 2 × 5 mm heat-treated AM, (a) and (b), and wrought, (c) and (d), maraging steel target plates impacted by armour piercing bullets, comparing the node splitting and element erosion failure techniques.

- The node splitting algorithm reproduced large, irregular fragments and radial cracks in target plates for the AM and wrought material, respectively, however, to a lesser extent than the severe fragmentation observed in experimental tests, especially for the AM material. The inclusion of AM-induced defects in the material model to capture fragmentation more accurately is left for further studies.

- Damage in the hard steel APM2 bullet core was included by use of the Cockcroft–Latham failure criterion, which was unable to capture fracturing of the bullet core as seen in experiments despite the accurate ballistic limit velocities achieved.
- Both structured and unstructured meshes paired with node splitting predicted ballistic limit velocities to within 4–5% of experiment. The unstructured mesh produced more natural crack patterns, whereas the structured mesh guided cracks along mesh grid lines.
- While node splitting gave ballistic limit velocity predictions within 2–3% of the experiment, element erosion yielded overestimations of roughly 11–13%. This discrepancy corresponds to an under-prediction of target plate fragmentation and cracking in the element erosion simulations.

REFERENCES

[1] Medvedev, A.E., Maconachie, T., Leary, M., Qian, M. & Brandt, M., Perspectives on additive manufacturing for dynamic impact applications. *Materials and Design*, **221**, 110963, 2022.

[2] Stavropoulos, P., *Metal Additive Manufacturing Technology Applications in Defense Organizations*, Springer International Publishing, pp. 1–35, 2021.

[3] Colorado, H.A., Cardenas, C.A., Gutierrez-Velazquez, E.I., Escobedo, J.P. & Monteiro, S.N., Additive manufacturing in armor and military applications: research, materials, processing technologies, perspectives, and challenges. *Journal of Materials Research and Technology*, **27**, pp. 3900–3913, 2023.

[4] Ngo, T., Kashani, A., Imbalzano, G., Nguyen, K. & Hui, D., Additive manufacturing (3D printing): A review of materials, methods, applications and challenges. *Composites Part B: Engineering*, **143**, pp. 172–196, 2018.

[5] Dehgahi, S., Alaghmandfard, R., Tallon, J., Odeshi, A. & Mohammadi, M., Microstructural evolution and high strain rate compressive behavior of as-built and heat-treated additively manufactured maraging steels. *Materials Science and Engineering: A*, **815**, 141183, 2021.

[6] Mooney, B., Kourousis, K. & Raghavendra, R., Plastic anisotropy of additively manufactured maraging steel: Influence of the build orientation and heat treatments. *Additive Manufacturing*, **25**, pp. 19–31, 2019.

[7] Costas, M., Edwards-Mowforth, M., Kristoffersen, M., Teixeira-Dias, F., Brøtan, V., Paulsen, C. & Børvik, T., Ballistic impact resistance of additive manufactured high-strength maraging steel: An experimental study. *International Journal of Protective Structures*, **12**(4), pp. 577–603, 2021.

[8] Edwards-Mowforth, M., Costas, M., Kristoffersen, M., Teixeira-Dias, F. & Børvik, T., On the ballistic perforation resistance of additively manufactured and wrought maraging steel: Experiments and numerical models. *International Journal of Impact Engineering*, **201**(8), 105271, 2025.

[9] Olovsson, L., Limido, J., Lacome, J.L., Hanssen, A.G. & Petit, J., Modeling fragmentation with new high order finite element technology and node splitting. *EPJ Web of Conferences*, **94**, 04050, 2015.

[10] Rakvåg, K., Børvik, T. & Hopperstad, O., A numerical study on the deformation and fracture modes of steel projectiles during taylor bar impact tests. *International Journal of Solids and Structures*, **51**(3), pp. 808–821, 2014.

[11] IMPETUS Afea, Home. https://www.impetus.no. Accessed on: Mar. 2025.

[12] Børvik, T., Hopperstad, O., Berstad, T. & Langseth, M., A computational model of viscoplasticity and ductile damage for impact and penetration. *European Journal of Mechanics – A/Solids*, **20**(5), pp. 685–712, 2001.

[13] Børvik, T., Dey, S. & Clausen, A., Perforation resistance of five different high-strength steel plates subjected to small-arms projectiles. *International Journal of Impact Engineering*, **36**(7), pp. 948–964, 2009.
[14] Dey, S., Børvik, T., Hopperstad, O. & Langseth, M., On the influence of fracture criterion in projectile impact of steel plates. *Computational Materials Science*, **38**(1), pp. 176–191, 2006.
[15] Kristoffersen, M., Costas, M., Koenis, T., Brøtan, V., Paulsen, C. & Børvik, T., On the ballistic perforation resistance of additive manufactured AlSi10Mg aluminium plates. *International Journal of Impact Engineering*, **137**, 103476, 2020.
[16] Bracq, A., Brest, J., de Sampaio, J., Moitrier, F. & Demarty, Y., Characterization and modelling of the mechanical behaviour of metal rings: Application to a brass bullet jacket. *Forces in Mechanics*, **4**, 100030, 2021.
[17] Cockcroft, M. & Latham, D., Ductility and the workability of metals. *Journal of the Institute of Metals*, **96**, pp. 33–39, 1968.
[18] Defense Technical Information Center, High Strain Rate Material Behavior. Technical Report ADA165214, Defense Technical Information Center, 1985.
[19] Ruggieri, C., Panontin, T.L. & Dodds, R.H., Numerical modeling of ductile crack growth in 3-D using computational cells. *International Journal of Fracture*, **82**, pp. 67–95, 1996.
[20] Geuzaine, C. & Remacle, J.F., Gmsh: A 3-D finite element mesh generator with built-in pre-and post-processing facilities. *International Journal for Numerical Methods in Engineering*, **79**(11), pp. 1309–1331, 2009.
[21] Recht, R. & Ipson, T., Ballistic perforation dynamics. *International Journal of Applied Mechanics (Trans ASME)*, **30**, pp. 384–390, 1963.